IL NUOVO CIMENTO Vol. 24 C, N. 3 Maggio-Giugno 2001

Non-equilibrium evolution of $HNO_3/H_2SO_4/H_2O$ stratospheric particles under multi-component diffusive condensation/evaporation regime(*)

V. Rizi and G. Visconti(**)

Dipartimento di Fisica, Università degli Studi
Via Vetoio, Località Coppito 67010, L'Aquila, Italy

(ricevuto il 5 Maggio 1999; revisionato l'8 Gennaio 2001; approvato il 23 Gennaio 2001)

Summary. — A box model is used to study the evolution of stratospheric $HNO_3/H_2SO_4/H_2O$ solution particles along temperature variations, which force the droplet ensemble far from the thermodynamic equilibrium. In the case of rapid temperature fluctuations, *i.e.* orographically forced lee waves, the model shows that the micron-sized droplets meet the conditions to become precursors of solid particles, mainly constituted of nitric acid hydrates. This paper examines how the particle size distributions and compositions are influenced by the presence of rapid temperature fluctuations, comparing model calculations along prescribed thermal histories. There results a remarkable dependence of the particle physical status (solid and/or liquid) on the presence of wave-like perturbations in the former thermal history of the air mass.

PACS 92.60.Mt – Particles and aerosols.
PACS 92.60.Hp – Chemical composition and chemical interactions.

1. – Introduction

The heterogeneous reactions induced by Polar Stratospheric Clouds (PSC) have a key role in the polar ozone depletion theories. These reactions activate the chlorine compounds which, mainly through the chlorine dimer cycle, become highly efficient in depleting ozone. The rates of heterogeneous reactions are treated through the use of *sticking coefficients*, γ, that is the fraction of the total number of collisions between a gas molecule and a particle surface that lead to a specific reaction. γ can change several orders of magnitude depending on the content of water and acid in the liquid droplets, and, in addition, it could be a factor 2 to 10 larger over liquid PSC surfaces, than solid.

(*) The authors of this paper have agreed to not receive the proofs for correction.
(**) E-mail: vincenzo.rizi@aquila.infn.it

Then a better understanding of the composition and state of the aerosol particle is needed for a correct assessment of their role.

The formation and the dynamics of the $HNO_3/H_2SO_4/H_2O$ liquid particles as well as their chemical partitioning are well known [1,2]. Our Aerosol Model (AM) has proved to be well suited to investigate the size distributions and the size-dependent acid weight fractions of the liquid $HNO_3/H_2SO_4/H_2O$ stratospheric aerosols evolving along different air mass thermal histories [3].

Observations of PSCs (*i.e.* Lidar [4]) show that these clouds often contain solid particles. The possible mechanisms forming the solid PSC particles and the processes affecting their composition at different thermodynamic stages are subjects of wide discussions [5-8]. Above the frost point, the solid PSCs are most likely composed of nitric acid hydrates, and such hydrates can be formed in the presence of severe temperature fluctuations encountered in mesoscale processes, *e.g.*, orographically forced lee waves [9].

This paper reports model studies of $HNO_3/H_2SO_4/H_2O$ liquid particle ensemble; performing very rapid temperature variations, the composition of these particles departs from the thermodynamic equilibrium, and meets the conditions to activate a freezing process, selective in the droplet radii, leading to the formation of solid phases. Namely the liquid-to-solid transition of the $HNO_3/H_2SO_4/H_2O$ stratospheric droplets can be efficient when the non-equilibrium particle composition is stochiometrically equivalent to that of nitric acid tri-hydrate (NAT, in weight 54% of HNO_3 and 46% of H_2O).

This work is organized as follows: Section **2** provides a brief overview of the Aerosol Model; this is followed by a description of the numerical simulations and a presentation of the results in sect. **3**. Section **4** provides the summary and a discussion of the results, and there we conclude speculating about the use of the model results as a tool for interpreting the local observations of polar stratospheric particles.

2. – Aerosol model

This aerosol model (AM) simulates the evolution of different categories of stratospheric aerosol particles in an air mass subject to an adiabatic temperature change, *i.e.* along Lagrangian trajectories. These particles are: the involatile (or solid) small particles which originate from the troposphere (we refer to these nuclei as Aitken particles, ATK), H_2SO_4/H_2O liquid droplets (WS), $HNO_3/H_2SO_4/H_2O$ liquid droplets (WSN), HNO_3 solid hydrates (NA-h), H_2SO_4 solid hydrates (SA-h) and ice particles.

Several physical processes are relevant for the formation and the dynamic evolution of an ensemble of sub-micron stratospheric particles [10]. The physical mechanisms accounted in AM are:

– heteromolecular homogeneous and heterogeneous nucleation of binary WS solution over ATK particles, of NA-h over SA-h and of ice over NA-h particles;

– homogeneous and heterogeneous freezing/melting nucleation of solid NA-h and SA-h from/to WS and WSN liquid solutions;

– diffusive condensation/evaporation of H_2SO_4, HNO_3 and H_2O to/from WS and WSN liquid particles and to/from ice, SA-h and NA-h solid particles;

– coagulation and sedimentation.

The parameterizations of these physical processes are extensively described in Rizi and Visconti [3]. We simply recall that each aerosol type or category (ATK, WS, WSN, SA-h, NA-h and ice particles) is represented by its own size distribution, $n_\alpha(r)$. $n_\alpha(r)\mathrm{d}r$ is the number density of type-α particles with radius between r and $r+\mathrm{d}r$, $r \in [0.01\,\mu\mathrm{m}, 100\,\mu\mathrm{m}]$ over $N = 100$ bins.

For the purposes of this work we mainly deal with the diffusive condensation/evaporation of H_2SO_4, HNO_3 and H_2O to/from WS and WSN liquid droplets and NA-h solid particles. The condensation/evaporation redistribute the particles of a single category over the radius space changing the size distribution.

2˙1. *Non-equilibrium diffusive condensation/evaporation of* $HNO_3/H_2SO_4/H_2O$ *liquid droplets*. – At the particle interface between two material phases (*i.e.* gas-liquid or gas-solid), there is a net flux of molecules from one phase to the other, and the rate of mass change can be described by

$$\frac{\mathrm{d}M_i}{\mathrm{d}t} = 4\pi D_i'(\rho_i - \rho_i^0 K(r))F(r), \tag{1}$$

where $\mathrm{d}M_i$ is the mass of the species i transported to or from the particles of radius r, between t and $t + \mathrm{d}t$; D_i' is the diffusion coefficient of the same species in the gas phase, corrected for the kinetic effects [11], ρ_i is the density of i-molecules in the gas phase, and $\rho_i^0 K(r)$ the corresponding saturation density corrected for the Kelvin effect. $F(r)$ includes corrections due to the heat flux induced by the transport of the molecules from one phase to the other [10].

In AM, the diffusive condensation/evaporation at gas-liquid and gas-solid interfaces is considered according to eq. (1). These rates can be used to predict the evolution of a particle ensemble. In the case of multi-component particles, the radius, r, of a droplet and the weight fractions, w_i, of the i-th component species evolve according to

$$\frac{\mathrm{d}r}{\mathrm{d}t} = \frac{1}{4\pi r^2 \rho_\mathrm{c}} \sum_j \frac{\mathrm{d}M_j}{\mathrm{d}t} \tag{2}$$

and

$$\frac{\mathrm{d}w_i}{\mathrm{d}t} = \frac{1}{(4/3)\pi r^3 \rho_\mathrm{c}} \left(\frac{\mathrm{d}M_i}{\mathrm{d}t} - w_i \sum_j \frac{\mathrm{d}M_j}{\mathrm{d}t} \right), \tag{3}$$

where ρ_c is the mass density of condensate, the summations are extended over all the different types of condensing/evaporating molecules, and in addition $\sum_j w_j = 1$.

The velocity of condensation is determined according to eqs. (1)-(3). We can consider an infinitesimal change of temperature, from T to $T + \mathrm{d}T$, and estimate the time needed to restore the equilibrium conditions. Equation (3) can be rewritten as

$$\frac{\mathrm{d}w_i}{\mathrm{d}t} \approx \left(A - \frac{w_i}{\tau} \right), \tag{4}$$

where A and τ are defined as

$$A = \frac{3D_i'(\rho_i - \rho_i^0 K(r))F(r)}{\rho_\mathrm{c} r^2}, \tag{5}$$

$$\tau = \frac{\rho_\mathrm{c}}{3\sum_j D_j'(\rho_j - \rho_j^0 K(r))F(r)} r^2 \tag{6}$$

(symbols and labels are the same of eq. (1)). τ is the lower limit for the time needed to reach the new value of w_i, because in a collection of droplets the flux of particles (ϕ_i)

between the different radii influences the single i-th bin evolution and the restoring of its equilibrium conditions. As an example, along the condensation, the smallest droplets take a long time to increase their radius: $\phi_i \cong 0$; the sub-micron particles can grow fast, then there is a net flux of particle to larger radii: $\phi_i < 0$; and finally in the larger bins of the size spectra, the net flux of particles is from smaller radii: $\phi_i > 0$. Then for a particle ensemble, eq. (4) should include an additional term which accounts for the particle flux between radii. In any case, the time constants for recovering the equilibrium become larger, and the departure from equilibrium is more pronounced.

The time constants, τ, are roughly proportional to the square of the particle radius, except for the smaller particles, for which the Kelvin, kinetic and latent heat effects are enhanced (in eq. (6), the diffusion coefficients, D'_j, increase, $K(r)$ and $F(r)$ become larger than 1). Therefore, the smaller and the larger particles need a longer time to reach the equilibrium. For the smallest droplets the Kelvin factor $K(r)$ can reach values between 1.2 and 1.5, which are sufficient to suppress their growth if the cooling or the temperature decline are not large enough; this means that the time for recovering equilibrium can be very long. A crude evaluation of eq. (6), for the conditions of the stratosphere ($T = 200\,\mathrm{K}$, $P = 50\,\mathrm{mbar}$, $[H_2O] = 5\,\mathrm{ppmv}$, $[HNO_3] = 10\,\mathrm{ppbv}$), gives τ of the order of tens of seconds for $0.1\,\mu$m droplets, and of hours for micron-sized particles. On the other hand, although the droplet composition can be far from equilibrium, H_2O is in equilibrium on time scales that are about 500 times lower than those of HNO_3 (it is roughly the ratio of the partial pressures).

In summary, from the point of view of a single particle evolution, after a temperature perturbation, the acid weight fractions promptly recover the equilibrium values at $0.1\,\mu$m size bin, while the transient to the equilibrium is quite slow at $0.01\,\mu$m, $1.0\,\mu$m and $10.0\,\mu$m size bins. Increasing the cooling rate means that the time period between two adjacent temperature perturbations decreases. Then if after the first perturbation the particles did not reach equilibrium (*i.e.*, the case of bins with longer τ), their composition continues to evolve away from equilibrium. For none of the size bins the condensation is fast enough to reach the new value of acid weight fractions when the temperature variation is more than $5\,\mathrm{K/day}$ [3]. Therefore the HNO_3 and H_2SO_4 contents of the real stratospheric droplets are often quite different with respect to those at equilibrium.

3. – Numerical simulations of the particle distribution and composition during a severe temperature fluctuation

We have considered an air mass that initially is characterized by an air pressure of 50 mbar and a temperature of 198 K, and the relevant gases have the following mixing ratios: 10 ppbv of HNO_3, 5ppmv of H_2O. H_2SO_4 can be regarded as an involatile solute, *i.e.* less than 0.01% of total H_2SO_4 is in the gas phase, the rest is dissolved in the aerosol droplets. This air mass also contains an ensemble of WS particles, typical of unperturbed polar stratosphere at about 200 K [12]: log-normal distributed, with a density of 10 particles cm^{-3}, a median radius of $r_0 = 0.08\,\mu$m, and a dispersion of $\sigma = 1.8$. The H_2SO_4 weight fraction of these particles is about 0.55 [13]. In our simulation the air mass isentropically cools down to 188 K with constant cooling of 10 K/day, and, at 193 K, the temperature falls down to 188 K with a cooling of about 120 K/day, and at the same rate is re-heated to continue the 10 K/day cooling (fig. 1). We can assume that this thermal history well represents the temperature profile of an air mass undergoing a temperature fluctuation caused by mountain-induced atmospheric gravity waves.

We have performed two model experiments: in the first (Rrun), the aerosols in the

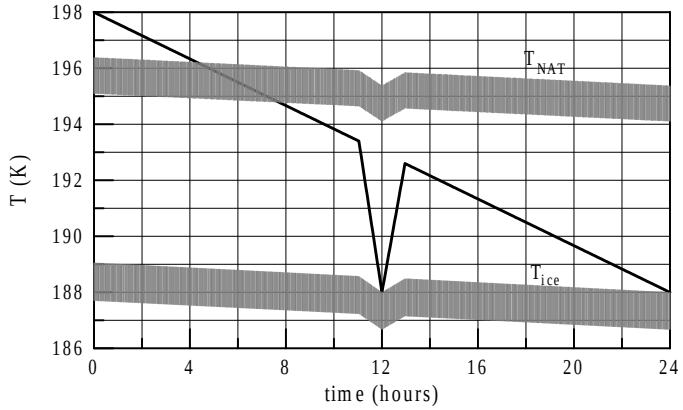

Fig. 1. – A thermal history (temperature *vs.* time) representing the temperature of an air mass exposed to a moderate cooling (10 K/day) and a temperature fluctuation typical of orographically forced gravity waves. The latter has been represented by a fast (120 K/day) dive and climb in the temperature profile. For the specified air mass (see text, 467 K potential temperature level, with 5 ± 1 ppmv of H_2O and 10 ± 2 ppbv of HNO_3), the equilibrium temperature of NAT formation (T_{NAT}) and the frost point (T_{ice}) are also indicated.

air mass remain liquid droplets (namely WSN aerosols), while in the second model run (Nrun) we assume that the particles with a composition close to NAT stochiometry become solid and continue to evolve as NAT particles.

3˙1. *Rrun experiment.* – The evolution of the size distribution of the liquid particles is reported in fig. 2: on cooling, the particles grow and the distribution is centered at larger radii. During the temperature fluctuation, the distribution closely follows the temperature variations shifting to larger radii on cooling and coming back to smaller radii on re-heating, then the particles continue to grow during the following slow cooling, removing HNO_3 and H_2O from the gas phase. The HNO_3 gas mixing ratio as a function of the time is shown in the top panel of fig. 3, the dashed line indicates the HNO_3 in gas phase during a cooling without temperature fluctuation. Along the temperature fluctuation more than 80% of total HNO_3 and about 4% of H_2O are condensed. A couple of hours after the temperature fluctuation, the gas composition of the air mass approaches the case of cooling without fluctuation. The characterization of the size distribution during the thermal history can be done looking at parameters like the total surface area (S) and volume (V) densities, and the effective radius (r_{eff}, which is the particle area-weighted mean radius that indicates the part of particle spectrum more contributing to the total surface area). These quantities are defined as

$$S = \int_0^\infty 4\pi r^2 n(r)\mathrm{d}r, \tag{7}$$

$$V = \int_0^\infty \frac{4}{3}\pi r^3 n(r)\mathrm{d}r, \tag{8}$$

$$r_{\mathrm{eff}} = 3\frac{V}{S} \tag{9}$$

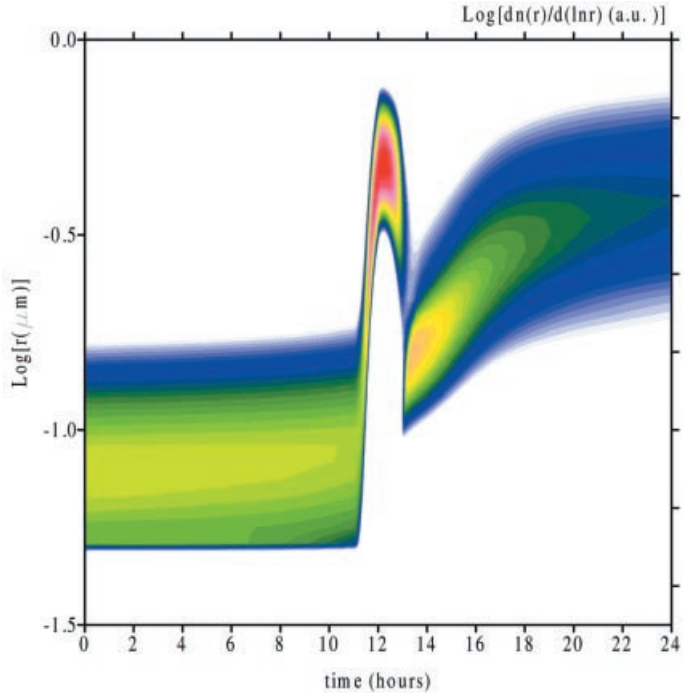

Fig. 2. – The false colour contour plot in this plate represents the size distribution of WSN particles during the Rrun simulation (only liquid particles). The radius axis is on log scale (*i.e.* -1 labels $0.1\,\mu$m). The differential particle density is reported in arbitrary units (blue = low values, red = high values); the total aerosol number density remains constant.

and S and r_{eff} are reported in the lower panels of fig. 3. The calculated surface area densities and the effective radius of the liquid particles promptly respond to the temperature fluctuation. The surface area density reaches its higher value ($26\,\mu\text{m}^2$ cm^{-3}) during the fluctuation. However, just after the severe cooling-heating, their values converge to the situation of an air mass performing cooling without fluctuation.

The evolution of the droplet composition is reported in fig. 4. The particles in $0.01\,\mu$m and $10.0\,\mu$m bins do not appreciably change their initial composition, the content of HNO_3 is quite low and its small increasing, as well as the decreasing of H_2SO_4, is due to the deliquescence by H_2O condensation. The $0.1\,\mu$m and $1.0\,\mu$m droplets show a composition that it is different from the equilibrium values, and, at about 191 K during the heating leg of the fluctuation, it is quite close to the NAT partitioning: in the $0.1\,\mu$m bin the HNO_3 and H_2SO_4 weight fractions are 0.53 and 0.006, respectively, and, in $1.0\,\mu$m bin, they reach 0.50 (HNO_3) and 0.05 (H_2SO_4). This behavior suggests that $0.1\,\mu$m droplets have the most favorable chance to become precursors of NAT solid particles, and there is a marginal possibility of freezing for $1.0\,\mu$m droplets [2].

3˙2. *Nrun experiment.* – In this simulation the aerosol particles evolve along the same thermal history of the previous experiment, in identical thermodynamic conditions. We include the freezing of the WSN droplets, assuming that the particles with a content of HNO_3 close to 54% and H_2SO_4 less than 0.1% of the droplet total mass become solid

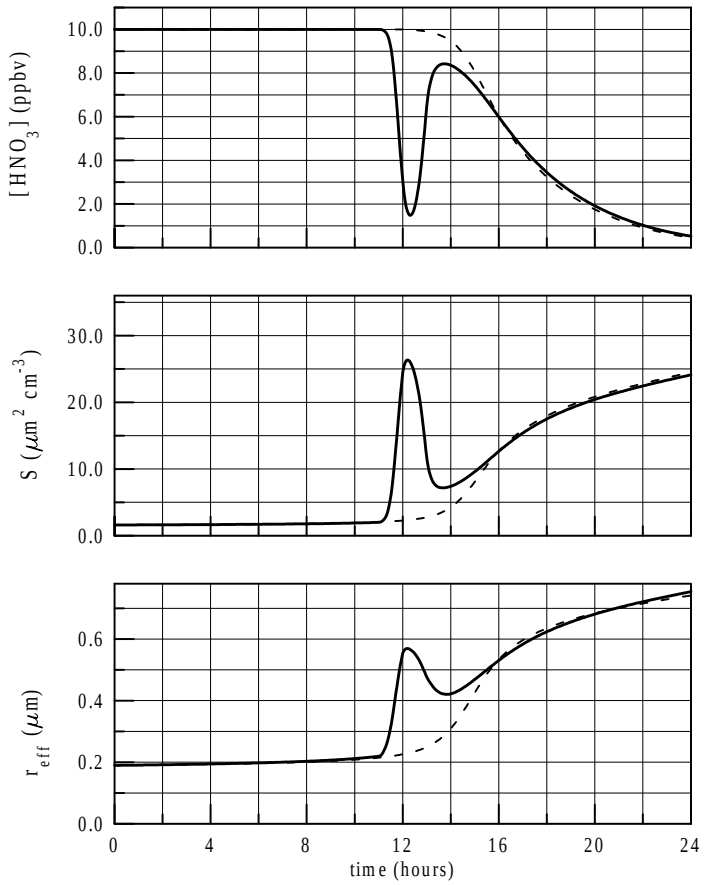

Fig. 3. – The evolution of HNO_3 gas mixing ratio (top panel, solid line), surface area density (middle panel, solid line) and effective radius (bottom panel, solid line) of the WSN liquid particles in Rrun simulation. The dashed lines represent the same quantities along an unperturbed temperature decline (*i.e.*, without fluctuation). Few hours after the fluctuation, Rrun experiment approaches the unperturbed cooling: at $T = 190\,\mathrm{K}$ ($t \sim 19\,\mathrm{hours}$), $S \cong 20\,\mu\mathrm{m}^2\ \mathrm{cm}^{-3}$, $r_{\mathrm{eff}} \cong 0.65\,\mu\mathrm{m}$ for both simulations.

NAT aerosols. The evolution of the particle ensemble is reported in the two color plates in fig. 5. The enhanced departure of droplet composition from equilibrium, during the temperature fluctuation, makes it possible that most of the particles in the radius range between 0.1 and $0.3\,\mu$m freezes as NAT.

On the slow cooling following the fluctuation, the NAT particles grow faster than the WSN droplets, and the NAT distribution appears bimodal, with the two modes peaked at about $0.35\,\mu$m and $0.8\,\mu$m. The WSN particles are distributed over a single mode centered at about $0.3\,\mu$m. The gas (HNO_3 and H_2O) concentrations, the surface area and volume density, and the effective radius of NAT and WSN aerosols along the thermal history are reported in fig. 6. The activation of NAT mode in the particle ensemble allows the condensation of almost the total available HNO_3 and the removal from gas phase is faster than in the Rrun experiment. The surface area and volume densities plotted in

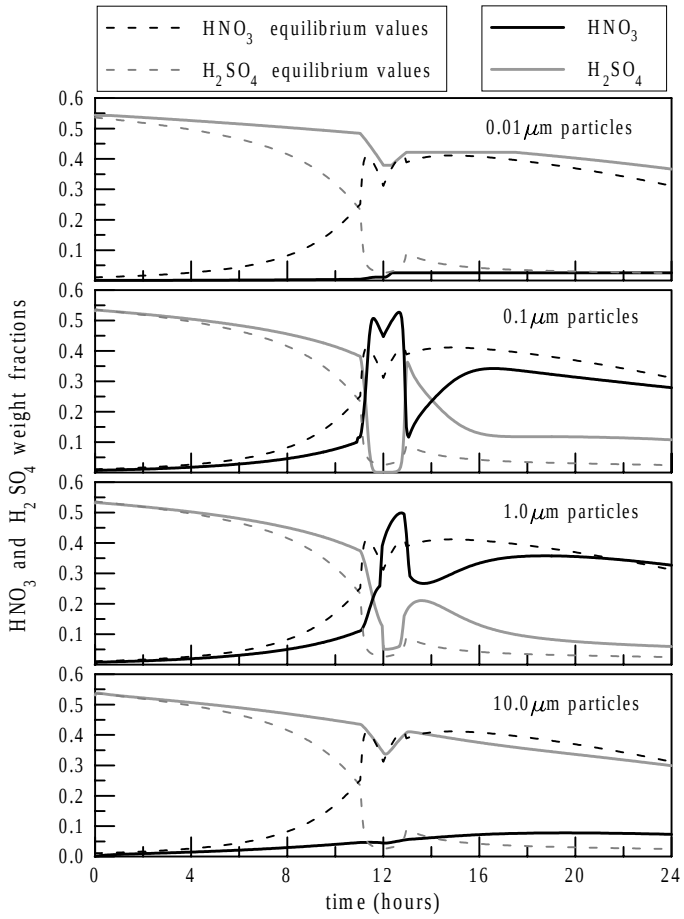

Fig. 4. – The H_2SO_4 (solid gray lines) and HNO_3 (solid black lines) weight fractions as a function of time in 0.01 μm, 0.1 μm, 1.0 μm, 10 μm particle bins along Rrun experiment. The equilibrium values are also indicated with dashed lines: H_2SO_4 (gray), HNO_3 (black).

fig. 6 suggest that most of the particle surface area and volume is concentrated in the NAT mode (that at larger radii) of the total size distribution. The rate of condensation in the Nrun experiment appears faster than in Rrun simulation; when, after the fluctuation, the temperature falls down to 191 K, more than 98% of total HNO_3 is condensed, and the particle size distributions approach a quasi-steady state. The total surface area density is about 20 μm^2 cm^{-3}, and more than 60% is due to the NAT particles; the total aerosol volume density reaches about 4 μm^3 cm^{-3}, and less than 20% relies in the WSN droplets. The effective radii of NAT and WSN particles are 0.74 μm and 0.4 μm, respectively.

4. – Discussion and conclusions

In this work, a Lagrangian Aerosol Model is applied to study the evolution of liquid particles, during severe temperature fluctuation, that can be encountered when lee wave activities propagate in the stratosphere.

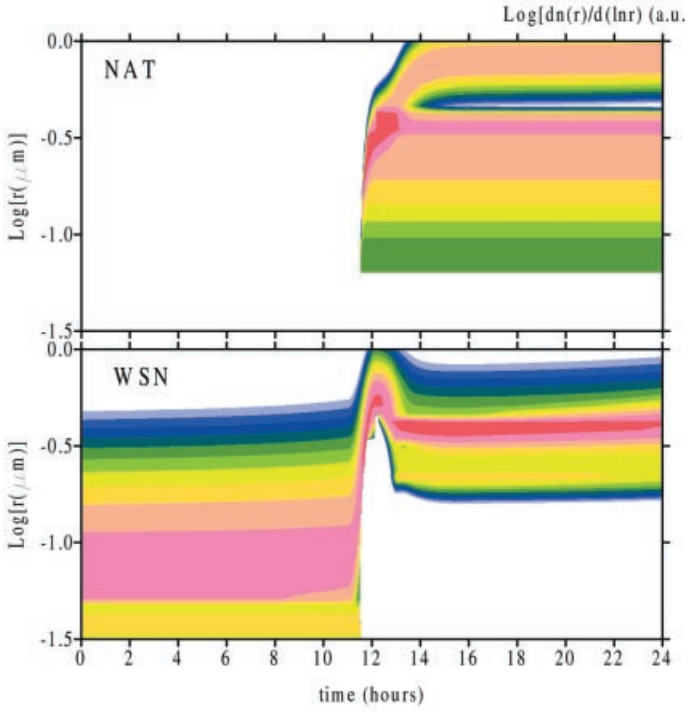

Fig. 5. – These two false colour contour plots represent the size distribution of NAT (top plate) solid particles and WSN liquid droplets (bottom plate) during the Nrun simulation. The temperature fluctuation acts as a motor drive in the formation of solid particles. The radius axis is on a log scale (*i.e.* -0.5 labels $0.32\,\mu$m). The differential particle density is reported in arbitrary units (blue = low values, red = high values); the total (NAT + WSN) aerosol number density remains constant. The particle number density reaches ~ 5.5 particles cm^{-3} and ~ 4.5 particles cm^{-3} for NAT and WSN aerosols, respectively.

We show that rapid temperature fluctuations cause liquid WSN aerosol to depart considerably from their equilibrium composition due to the diffusively hindered uptake of HNO_3. The small droplets (between 0.1 and $0.3\,\mu$m) can approach binary HNO_3/H_2O concentrations with the chance to freeze as nitric acid hydrates. Our model shows that the particles with radius of about $0.1\,\mu$m, during a fast cooling, and the micron-sized particles, during a subsequent rapid heating, meet the conditions to become the precursor of NAT solid particles, according to the mechanism suggested by Meilinger *et al.* [14]. This process has been included in our aerosol model: the calculations show that a moderate cooling strongly deviate the particle composition from equilibrium, and the presence of a severe temperature fluctuation can originate certain condition favourable to the liquid-to-solid transition.

In the simple scenario (Nrun) used for representing the occurrence of a lee wave, most of the aerosols become NAT particles, and the HNO_3 rate of condensation appears faster than in the case of cooling without temperature fluctuation. It is evident that the NAT particles, in this case, grow faster than the remaining WSN droplets. The reason of such a difference is that the NAT aerosols are activated below their equilibrium temperature, so the saturation of HNO_3/H_2O vapor can largely exceed the NAT saturation value.

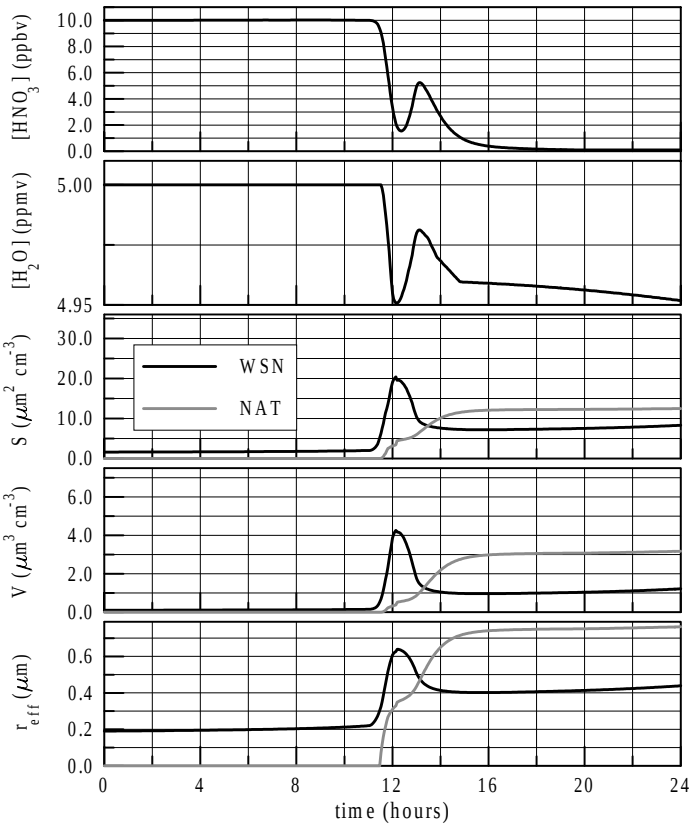

Fig. 6. – The HNO_3 and H_2O gas mixing ratios (top panels), surface area densities (middle panel), particle volume densities and the effective radii (bottom panels) of the WSN liquid particles (black line) and NAT (gray line) as a function of time during Nrun simulation. Note that 4 hours after the temperature fluctuation, the size distribution parameters reach a quasi-steady state.

And, in addition, the HNO_3 and H_2O gases preferentially condense over NAT particles because their radii span a region (0.1–1.0 μm) where the Kelvin, kinetic and latent heat effects as well as the diffusively hindered uptake are quite moderate (see subsect. **2**˙1).

The remote and/or *in situ* PSC observations capture the aerosol particles at a particular stage of their evolution. The local properties of PSC particles are strictly connected to the former thermodynamic evolution. As a consequence, a correct interpretation of the data must take into account the thermal histories of the sampled air masses. As an example Lidar measurements require such interpretation. Many of the observations can be understood by taking into account synoptic scale fluctuations of air parcel temperatures as revealed by trajectory analyses (*i.e.* Rizi *et al.*, [15]). But in some occasions there is a poor correlation between the local observation and the available synoptic thermal histories of the sampled air masses. Several PSC Lidar measurements reported by Stein *et al.* [4] show that the observations are consistent with the presence of a limited number of solid particles, when the synoptic scale conditions suggested the presence of liquid droplets. Probably, in these cases, mesoscale fluctuations, not resolved by the large-scale analysis, are present along the air mass thermal histories.

Referring to our simulations, a Lidar sampling at a wavelength of 532 nm of the air mass at $t \sim 19$ hours of the thermal history gives backscattering coefficients (proportional to the total surface area density of the measured aerosols) and depolarization ratios (roughly proportional to the relative abundance of solid particles in the aerosol ensemble) that are about $0.4 \cdot 10^{-6}\,\mathrm{m}^{-1}\,\mathrm{sr}^{-1}$ and 0%, respectively, for Rrun experiment, and about $0.5 \cdot 10^{-6}\,\mathrm{m}^{-1}\,\mathrm{sr}^{-1}$ and more than 10% for Nrun.

Rizi *et al.* [3] have outlined simple criteria, based on air mass synoptic trajectories, for the first analysis of remote and/or *in situ* observations of stratospheric particles:

– if the air mass has cooled slowly from a temperature above the SAT melting point, but remains above the ice point, it should contain only liquid particles (typically moderate scattering coefficients and no depolarization);

– solid particles should be present if the air temperature is, or has recently been, below the ice point (high scattering coefficients and high depolarization);

– solid particles may be present in air at temperatures above the ice point, if the air has cooled very rapidly (more than 20 K/day) down to 190 K and subsequently re-warmed, or if the temperature has oscillated, with maxima lower than the SAT melting point and minima close to the ice point (moderate scattering coefficients and high depolarization).

When these criteria generate a poor correlation between the measurements and the thermal histories, it is likely that the analysis should consider the presence of small-scale perturbations.

In conclusion, PSC data analysis should try to recognize these situations (*e.g.*, Tsias *et al.* [8] were able to give a successful explanation of a Lidar PSC observation clearly formed by the presence of lee waves). But in attempting to represent the chemistry of the stratosphere the relative occurrence of PSC in solid and liquid phase should be modelled, because it can have effects on the rates of chlorine activation via the heterogeneous chemistry [16], and on the denitrification of polar winter stratospheres. The mountain-induced mesoscale temperature perturbations can become the dominant drive for the formation of solid PSC in Arctic, where the stratospheric temperatures sporadically reach the ice frost point [9].

* * *

This work was part of SAONAS (Stratospheric Aerosols and Ozone in Northern And Southern hemispheres) in Winter 1996/1997 and of APE (Airborne Polar Experiment) in Winter 1996/1997. Part of this work was supported by the European Community - DG XII - under contracts No. EV5V-CT93-0355, ENV4-CT95-0090 and ENV4-CT95-0143.

REFERENCES

[1] Carslaw K. S., Peter T. and Clegg S. L., *Rev. Geophys.*, **37** (1997) 125.
[2] Koop T., Carslaw K. S. and Peter T., *Geophys. Res. Lett.*, **24** (1997) 2199.
[3] Rizi V. and Visconti G., *J. Aerosol Sci.*, **30** (1999) 1095.
[4] Stein B., Wedekind C., Wille H., Immler F., Müller M., Wöste, Del Guasta M., Morandi M., Stefanutti L., Antonelli A., Agostini P., Rizi V., Redaelli G., Mitev V., Matthey R., Kivi R. and Kyrö E., *J. Geophys. Res.*, **104** (1999) 23983.
[5] Tabazadeh A., Toon O. B. and Hamill P., *Geophys. Res. Lett.*, **22** (1995) 1725.
[6] Tabazadeh A. and Toon O. B., *J. Geophys. Res.*, **101** (1996) 9071.
[7] Tabazadeh A., Toon O. B., Gary B. L., Bacmeister J. T. and Schoeberl M. R., *Geophys. Res. Lett.*, **23** (1996) 2109.

[8] Tsias A., Prenni A. J., Carslaw K. S., Onash T. P., Luo B. P., Tolbert M. A. and Peter T., *Geophys. Res. Lett.*, **24** (1997) 2303.
[9] Carslaw K. S., Peter T., Bacmeister J. T. and Eckermann S. D., *J. Geophys. Res.*, **104** (1999) 1827.
[10] Pruppacher H. R. and Klett J. D. (D. Reidel Publishing Compay, Holland) 1980.
[11] Kulmala M., Vesala T. and Wagner P. E., *Proc. R. Soc. London.*, **441** (1993) 589.
[12] Dye J. E., Baumgardner D., Gandrud B. W., Kawa S. R., Kelly K. K., Loewenstein M., Ferry G. V., Chan K. R. and Gary B. L., *J. Geophys. Res.*, **97** (1992) 8015.
[13] Zhang R., Wooldridge P. J. and Molina M. J., *J. Phys. Chem.*, **97** (1993) 8541.
[14] Meilinger S. K., Koop T., Luo B. P., Huthwelker T., Carslaw K. S., Krieger U., Crutzen P. J. and Peter T., *Geophys. Res. Lett.*, **22** (1995) 3031.
[15] Rizi V., Redaelli G., Visconti G., Masci F., Wedekind C., Stein B., Immler F., Mielke B., Rairoux P., Woste L., Del Guasta M., Morandi M., Catagnoli F., Balestri S., Stefanutti L., Matthey R., Mitev V., Douard M., Wolf J. P., Kyro E., Rummukainen M. and Kivi R., *J. Atmos. Chem.*, **32** (1999) 165.
[16] Carslaw K. S. and Peter T., *Geophys. Res. Lett.*, **24** (1997) 1743.